Received: 11 July 2023 | Revised: 11 August 2023 | Accepted: 13 August 2023

DOI: 10.1002/pc.27689

RESEARCH ARTICLE

Polymer COMPOSITES WILEY

Lubrication mechanism of polyimide/V_2CT_x MXene composites based on surface chemistry

Lanyu Jin[1] | **Xinrui Wang**[1] | **Yufei Huang**[1] | **Guojing Chen**[1] | **Haosheng Pang**[2] | **Xuan Yin**[3] | **Chunpeng Chai**[1]

[1]School of Materials Science and Engineering, Beijing Institute of Technology, Beijing, China

[2]Chinese Aeronautical Establishment, Beijing, China

[3]College of Mechanical and Electrical Engineering, Beijing University of Chemical Technology, Beijing, China

Correspondence
Xuan Yin, College of Mechanical and Electrical Engineering, Beijing University of Chemical Technology, Beijing 100029, China.
Email: yinxuan@mail.buct.edu.cn

Chunpeng Chai, School of Materials Science and Engineering, Beijing University of Chemical Technology, Beijing 100029, China.
Email: chaicp@bit.edu.cn

Funding information
Liaoning Key Laboratory of Aero-engine Materials Tribology, Grant/Award Number: LKLAMTF202304; National Natural Science Foundation of China, Grant/Award Number: 52075284; Tribology Science Fund of State Key Laboratory of Tribology in Advanced Equipment, Grant/Award Number: SKLTKF21B09

Abstract

A series of polyimide (PI)/V_2CT_x MXene composites was synthesized via polyamide acids (PAA) and two-dimensional (2D) V_2CT_x MXene obtained by etching precursor V_2AlC. PI/V_2CT_x MXene composites with different mass ratios were obtained by blending and heating with PAA. The results showed that V_2CT_x MXene has excellent dispersion in PI. In particular, V_2CT_x MXene exhibited excellent friction reduction and anti-wear properties as a solid lubricant additive, and the wear rate (WR) was reduced by 43.2% by incorporating only 0.8 wt% of V_2CT_x MXene in the pristine PI and 71.9% by incorporating 1.2 wt%. Scanning electron microscopy (SEM) and x-ray photoelectron spectroscopy (XPS) analyses showed that the continuous transfer film consisting of a high proportion of tribo-chemical products formed on the contact surface is significant to improve the lubrication performances of the PI composites. This work broadens the application of MXene in the field of tribology and contributes to energy conservation and sustainable development of human society.

Highlights

- The tribological properties could be tuned by changing the ratio of PI to V_2CT_x MXene.
- The WR of PI composites was reduced by 71.9% with incorporating 1.2 wt% of V_2CT_x MXene.
- The formation of transfer films on the contact surface is significant for improving anti-wear of PI.

KEYWORDS
composites, functional polymers, lamellar, structure–property relations, surface

1 | INTRODUCTION

Polymer-based composites have received a lot of attention in anti-friction and anti-wear engineering materials via their lightweight and excellent self-lubricating properties. Polyimide (PI) has excellent mechanical properties and good thermal- and chemical stability,[1] and plays a fundamental role in many high-tech applications such as aero-engines, aerospace vehicles, the microelectronics industry, and precision machinery.[2–7] However, the application of the pristine PI in solid lubricant materials is limited by the high coefficient of friction (COF) and the poor wear resistance.[8,9] Therefore, many types of lubricant additives have been incorporated into PI to improve its frictional wear resistance. In particular, the usage of two-dimensional (2D) materials such as

graphene, graphite, molybdenum disulfide (MoS_2), and boron nitride, is filled into the polymer matrix as solid lubricant additives, which is an effective way to reduce COF and the wear rate (WR).[10–12] The lubrication mechanism can be attributed to the relative sliding of 2D solid lubricant additives. This will act as an energy absorber and vibration dampener. Furthermore, a transfer film is gradually formed on the contact surfaces, preventing direct contact between the lubricant material and the friction substrate. However, usually van der Waals forces exist between the nanosheets of 2D materials, which makes the 2D materials, when used as additives, tend to aggregate in the polymer matrix, resulting in poor dispersion and abrasive debris, which affects the stability and densification of the transfer film on the friction substrate. The following issues need to be addressed to obtain 2D material-modified PI-based composites with excellent tribological properties: (1) Improving the dispersion of 2D material in the PI matrix and its interfacial compatibility with the matrix. (2) The modified composites need to have the ability to form continuous transfer films. The general way to solve the above problems is to apply special treatments to the surface of 2D materials. However, not only does this treatment complicate the process of introducing lubricating fillers, but it enhances filler dispersion and affinity between the substrate and filler to a limited extent.[13]

MXene, first reported in 2011, is a class of 2D transition metal carbides,[14] which possesses good thermal stability and excellent mechanical strength,[15,16] and exhibits weak interlayer interactions, making MXene more susceptible to interlayer sliding. In particular, MXene naturally possesses surface functional groups such as —F and —OH, which can significantly enhance its bonding with the substrate and improve the dispersion of MXene in the substrate. All these make MXene a lubricant additive of great interest.[17] It has been shown that MXene has a low sliding energy barrier using molecular dynamics simulations, and density flooding theory calculations. A large number of experiments have also confirmed that MXene additives can improve the tribological properties of the substrate.[18–20] For example, Liang[21] added $Ti_3C_2T_x$ MXene solid lubricant additive to polyurea (PUA)/PI copolymer, and the COF of PUA/6PI/$Ti_3C_2T_x$ composites decreased by 59.1% and 58.6% compared to the pure PUA/6PI at 25 and 100°C, respectively.

However, $Ti_3C_2T_x$ MXene is easily oxidized in the air to the more stable TiO_2 and generates carbon monomers,[21] which scratches the transfer film and increases the wear and COF of the composite, while V_2CT_x MXene is only oxidized and decomposed at higher temperatures.[22] Therefore PI/V_2CT_x MXene has theoretically higher thermal and chemical stability than PI/$Ti_3C_2T_x$ MXene, which is beneficial for the improvement of friction and wear resistance. In addition, it has been shown that the carbide Nb_2C MXene of the VB subgroup element Nb has a higher density of surface dipole moments and a more uniform distribution of electron clouds than $Ti_3C_2T_x$ MXene, and the carbide V_2CT_x MXene of the same VB subgroup V is likely to exhibit similar properties, which are reflected macroscopically that V_2CT_x MXene has a lower COF and adhesion than $Ti_3C_2T_x$ MXene.[23]

In this study, V_2CT_x MXene was used for the first time as a solid lubricant additive for PI to improve the friction and wear resistance of the PI. The lamellar V_2CT_x MXene was first obtained by HF etching of V_2AlC, and the polyamide acids (PAA)/V_2CT_x composite was obtained by co-blending with PAA, and the PI/V_2CT_x MXene composite was obtained after heating. The surface morphology of the composites and slipping surfaces were observed by scanning electron microscopy (SEM) before and after the friction test, supplemented by x-ray photoelectron spectroscopy (XPS) to analyze the microscopic lubrication mechanism. As a result, the friction and wear resistance of PI/V_2CT_x MXene composites with different proportions of V_2CT_x MXene additives were investigated comparatively.

2 | EXPERIMENT SECTION

2.1 | Materials and methods

2.1.1 | Preparation of lamellar V_2CT_x MXene

The synthesis process of lamellar V_2CT_x MXene was as follows: (1) 2.1 g of LiF powder was dissolved in 15 mL of 40% HCl and stirred for 15 min; (2) 1.1 g of V_2AlC MAX phase powder (purity >99%, 200 mesh, purchased from Jilin One–One Technology Co., Ltd.) was added in batches and etched at 90°C with stirring (500 rpm) for 48 h; (3) The etched V_2CT_x was repeatedly washed with deionized water by centrifugation (3500 rpm, 5 min) and filtration until the supernatant was neutral; (4) The prepared V_2CT_x was collected by filtration and dried under vacuum at 60°C for 12 h to obtain the lamellar V_2CT_x MXene.

2.1.2 | Synthesis of PI/V_2CT_x MXene composites

Weigh 4.0048 g of 4,4-diamino diphenyl ether (ODA) and add to 50 mL of N, N-dimethylacetamide (DMAc) and sonicate for 30 min until completely dissolved. Weigh an equimolar ratio of 4.3624 g of homophthalic

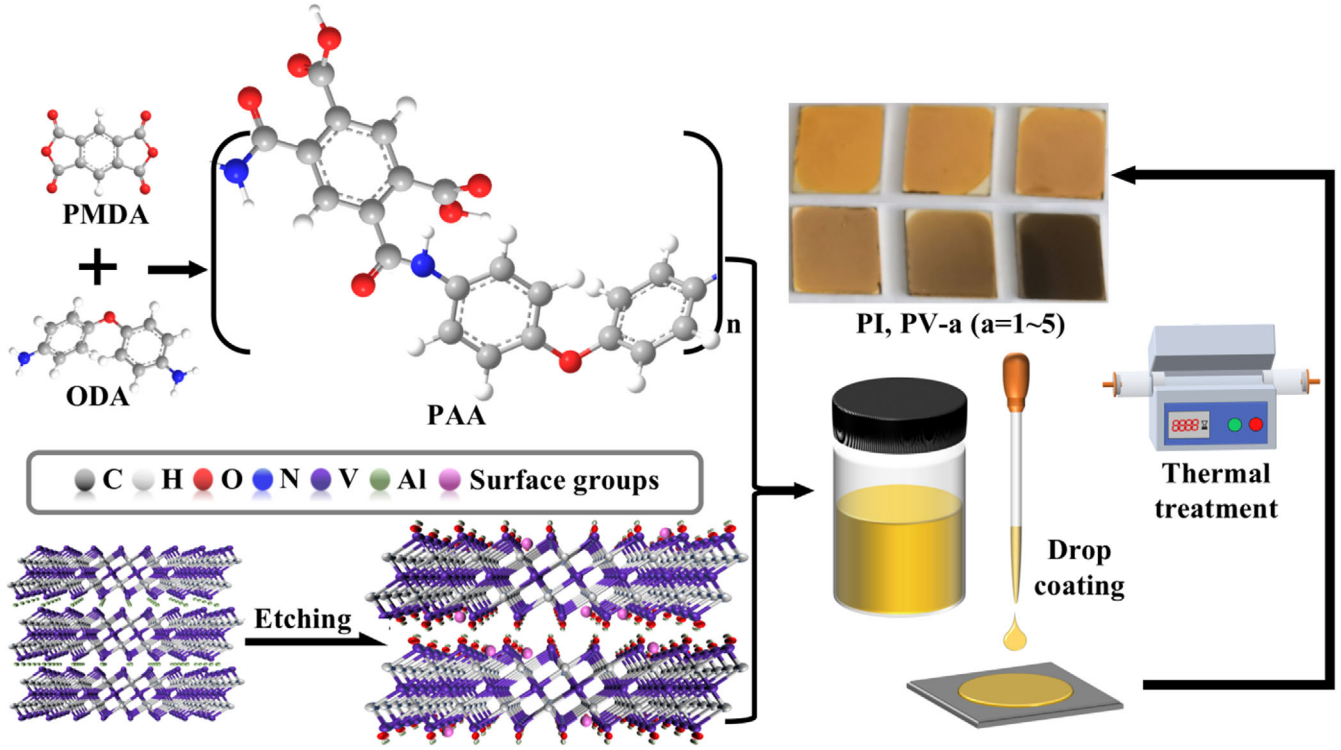

FIGURE 1 Schematic diagram of the preparation process.

dianhydride (PMDA) into the ODA solution and react in an ice water bath for 3 h to obtain a 12% solids solution of PAA.

Different masses of V_2CT_x were weighed separately, ultrasonically dispersed in a certain amount of DMAc, and subsequently added to 8.0 g PAA solution, stirred at high speed for 30 min, and then uniformly coated on 304 steel plates and dried under vacuum at 60°C for 8 h. After that, they were placed in a tube furnace to be completely thermally oxidized according to a specific heating procedure to finally obtain PI/V_2CT_x MXene composites with V_2CT_x of 0.4, 0.8, 1.2, 1.6, and 2.0 wt%, denoted as PV-a ($a = 1 \sim 5$), respectively. The pristine PI was prepared in the same way (i.e., adding V_2CT_x as 0 wt%) to be used for comparison. A schematic diagram of the preparation process of the composites is shown in Figure 1.

2.2 | Characterization

The chemical structures of PI and PAA were characterized by Fourier transform infrared spectroscopy (FT-IR, Affinity-1S). The preparations V_2AlC and V_2CT_x were analyzed by x-ray diffraction (XRD, Rigaku, Smart Lab SE, Japan) with a scan rate of 2°/min, using Cu K_α radiation with $\lambda = 1.5406$ Å.

The COF and WR of the polymer matrix and its composites were measured on a multifunctional, ball-on-disc tribometer (BOD, MS-M9000, China) to evaluate their tribological properties. Before the tribological tests, the steel balls (GCr15, diameter = 4 mm, Yiwu Hongzhou Trading Co., Ltd.) were thoroughly cleaned with ethanol in an ultrasonic bath for 30 min and the tribological tests were carried out at 50 r/min. Referring to previous experience,[24] the duration of each test is 30 min and the test is repeated at least 3 times under each condition. The COF during sliding was recorded online. 3D white light interferometry (ZYGO NewView) was used to characterize the surface morphology of the material before and after the friction test. The wear volume of the composite material was calculated by the 3D white light interferometry. The WR of the specimen is calculated by the formula

$$\mathrm{WR} = \frac{S \times C}{L \times D},$$

where L is the load (N), D is the sliding distance (m), S derived from the 3D white light interferogram is the area of the abrasion cross-section (mm^2), and C is the length of the annular abrasion (mm).

To investigate the lubrication mechanism of the composites, the tribo-affected surfaces of PI and PI/V_2CT_x composites after sliding with steel ball were characterized by field emission SEM (FEI Quanta 250) and XPS (PHI QUANTERA-II SXM, Japan). An energy dispersive

spectrometer (EDS) equipped with SEM was used to obtain elemental maps.

3 | RESULTS AND DISCUSSION

3.1 | Analysis of the structure of MXene

To confirm the successful preparation of V_2CT_x, XRD, SEM, and Transmission Electron Microscopy (TEM) characterization was performed and the results are shown in Figure 2. As shown in Figure 2B, most of the characteristic diffraction peaks of V_2AlC at 13.45° (002) and 41.24° (103) disappeared after etching. This indicated that the Al layer was removed during the etching process. New diffraction peaks appeared at 7.42° (002), 24.89° (006), and 35.55° (021), indicating that most of the V_2AlC has been converted into V_2CT_x MXene. SEM images show that V_2AlC shows a 3D structure with tight interlayer stacking. However, after etching, the resulting V_2CT_x has a distinct 2D lamellar structure with increased layer spacing. In addition, the interlayer spacing of V_2CT_x is 0.9634 nm as derived from the TEM image (Figure 2C), which indicates that V_2CT_x has a high purity.

For V_2CT_x, the ratio of the fitted peak V(II) is as high as 32.8% (Figure S1b$_3$); the ratio of V and O atoms of V_2CT_x is 0.417 (Figure S1a); and the ratio of F atoms on the surface of V_2CT_x MXene is 0.66% (16.6%). The above indicates that V_2CT_x is pristine and contains —OH, —F, and other surface groups.

3.2 | Structures of PI and PI/V_2CT_x composite

Figure S1c shows the chemical structure of PI. It can be seen that the asymmetric and symmetric telescopic vibrational peaks of C═O in PI appear at 1778 and 1717 cm^{-1}, respectively, proving the occurrence of thermal imidization. Meanwhile, the bending vibration peak of C═O appeared at 721 cm^{-1} and the telescopic vibration peak of C—N appeared at 1368 cm^{-1}. The telescopic vibrations of N—H (gained from —NH_2), O—H (gained from —COOH) (2900 ∼ 3200 cm^{-1}), the vibration of C═O (COOH) (1680 cm^{-1}), and the vibration peak of C—NH (CONH) (1550 cm^{-1}) in PAA all disappeared. This indicated the successful preparation of PI.

XPS analysis of PI/V_2CT_x composites was performed to further investigate the microscopic effects of the addition of V_2CT_x on the PI matrix. XPS spectra of V_2CT_x are shown in Figures S1a,b, where the termination group formed on the surface during the etching process, signal the presence of O elements in V_2CT_x. Compared to the pristine PI, N elements were detected in the PV-2 composite and the signal intensity of C1s was significantly higher (Figure S1d). The high-resolution V2p spectra can be deconvoluted into three components[25] as shown in Figure S1b$_3$: V-C/V(II) (513.94 eV, V $2p_{3/2}$/521.14 eV, V $2p_{1/2}$), V(III) (516.04 eV, 521.94 eV) and V(IV) (517.54 eV, 525.14 eV). As shown in Figure S1e,f$_1$, when V_2CT_x was added to the PI matrix, the signal of the C-V bond appeared in the C 1s spectrum. All of the above indicate that V_2CT_x was introduced into the PI-based in situ.

3.3 | Performances of PI and PI/V_2CT_x composite

In terms of tribological properties, Figure 3A shows the variation of COF with sliding time (distance) for the pristine PI and its composites under a load of 5 N. Influenced by the roughness of the contact surface, it can be observed that all specimens showed an intensive friction at the initial stage of the test, which is considered a running-in period.[26] We assumed that the frictional heat generated during sliding increases the temperature, causing the PI to gradually enter a highly elastic state. The adhesion of PI to the steel ball will increase, and the excessive viscoelastic material may also reduce the easy shear property of the sliding interface. Therefore, the COF of pristine PI is higher than that of PI/V_2CT_x.[21,27] Due to the addition of an appropriate amount of V_2CT_x MXene to improve the stability of the PI, the surface of composite is smoother during the friction process and the COF is lower than that of the pristine PI. Overall, the PI/V_2CT_x composite containing 0.8 wt% V_2CT_x (i.e., PV-2) had the lowest COF. In this case, the added V_2CT_x has interlayer slip and moves in concert with the PI molecular chain, which serves to increase lubrication and reduce friction. In addition, the small amount of V_2CT_x added is less likely to cause agglomeration, resulting in a larger specific surface area of V_2CT_x, which is also conducive to increased lubrication. The WR of the pristine PI, PV-1, PV-2, PV-3, PV-4, PV-5 under 5N load is 1.392×10^{-5}, 1.373×10^{-5}, 0.791×10^{-5}, 0.391×10^{-5}, 0.978×10^{-5}, and 1.552×10^{-5} $mm^3/(N \cdot m)$. It can be seen that the addition of V_2CT_x plays an important role in reducing wear and enhancing the lubricating properties of the polymer matrix. As the mass fraction of the V_2CT_x additive in the PI-based increased, the WR of the composites first decreased significantly and then increased. Among them, the WR of PV-2 and PV-3 were 43.2% and 71.9% lower than that of the pristine PI, respectively (Figure 3B).

Figure 4A–C shows the SEM image of the contact surface of the bearing steel ball. When the pristine PI was

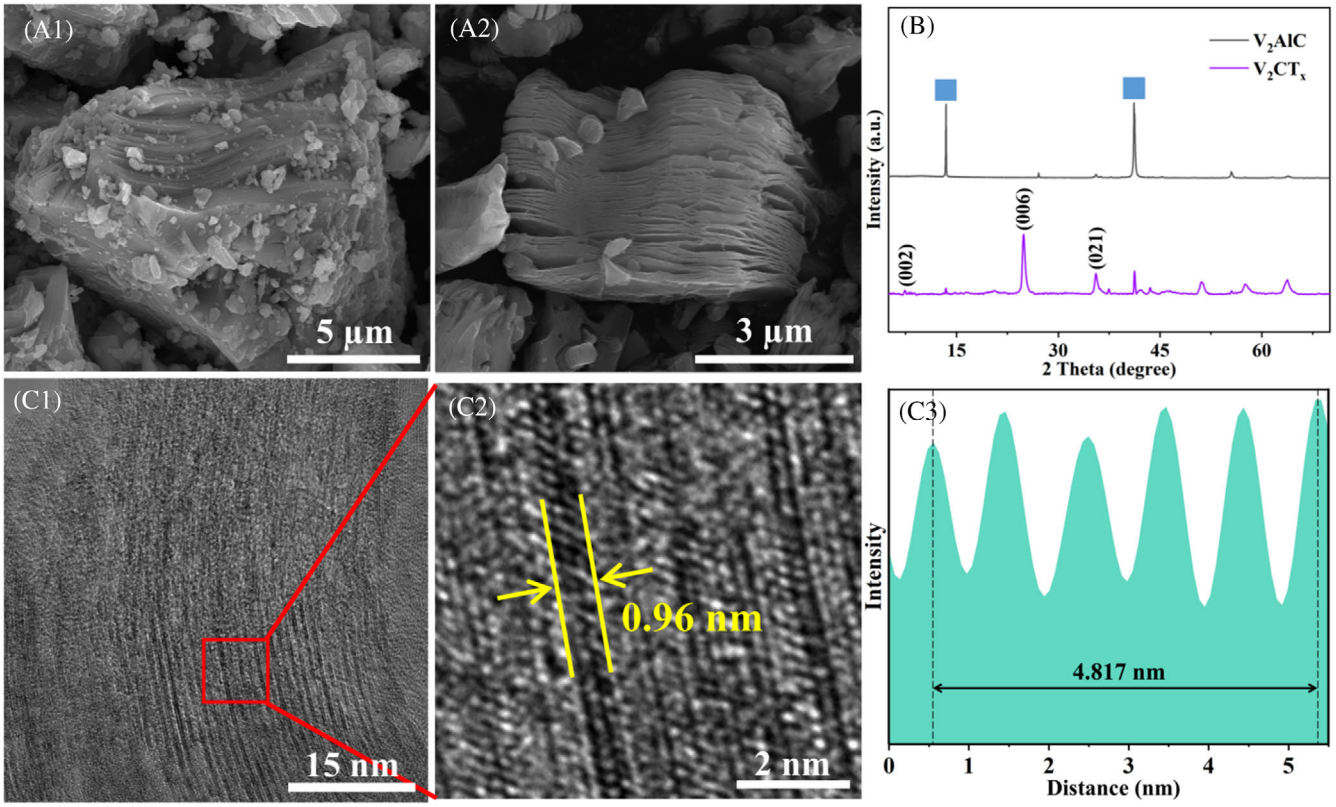

FIGURE 2 Scanning electron microscopy images of (A_1) V_2AlC, (A_2) V_2CT_x. (B) X-ray diffraction characterization of V_2CT_x and V_2AlC. (C_1, C_2) TEM maps of V_2CT_x, (C_3) layer spacing of V_2CT_x.

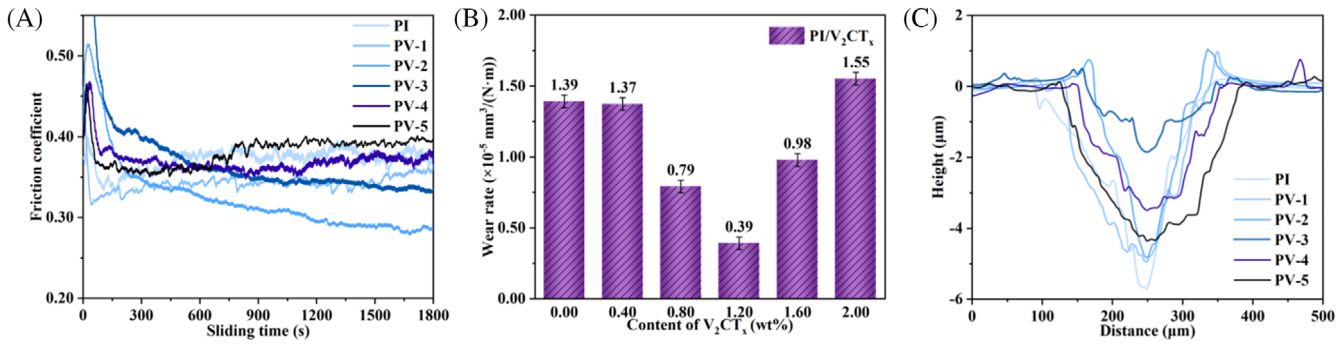

FIGURE 3 (A) Coefficient of friction curves with time for polyimide (PI) and PV-a ($a = 1 \sim 5$). (B) Average wear rate (calculated from C). (C) Width-depth curves of abrasion marks for PI and PV-a ($a = 1 \sim 5$).

the specimen, a large number of abrasive chips moved onto the steel balls (Figure 4A). When the mass fraction of V_2CT_x additive reached 0.8 wt%, the transfer film formed on the contact surface was relatively continuous (Figure 4B). As the content of V_2CT_x increased to 1.6 wt %, the transfer film showed a punctiform dispersion on the frictional subsurface of steel ball (Figure S2b). This is due to the previously generated nano-micro-bearings[28] being wrapped and aggregated with each other, forming large granular abrasive chips, which tend to cause deformation of the contact surface. The friction subsets were subjected to continuous impact during the reciprocal friction test, so these abrasive chips can affect the formation of continuous transfer films. Figure 4D–F shows the 3D morphology of the contact surface of the bearing steel ball, which reflects the wear situation consistent with the analysis obtained in Figure 4A–C.

The 3D white-light interference morphology of the wear marks of PI composites is shown in Figure 5D–F. From Figure 5D, it can be observed that the surface of

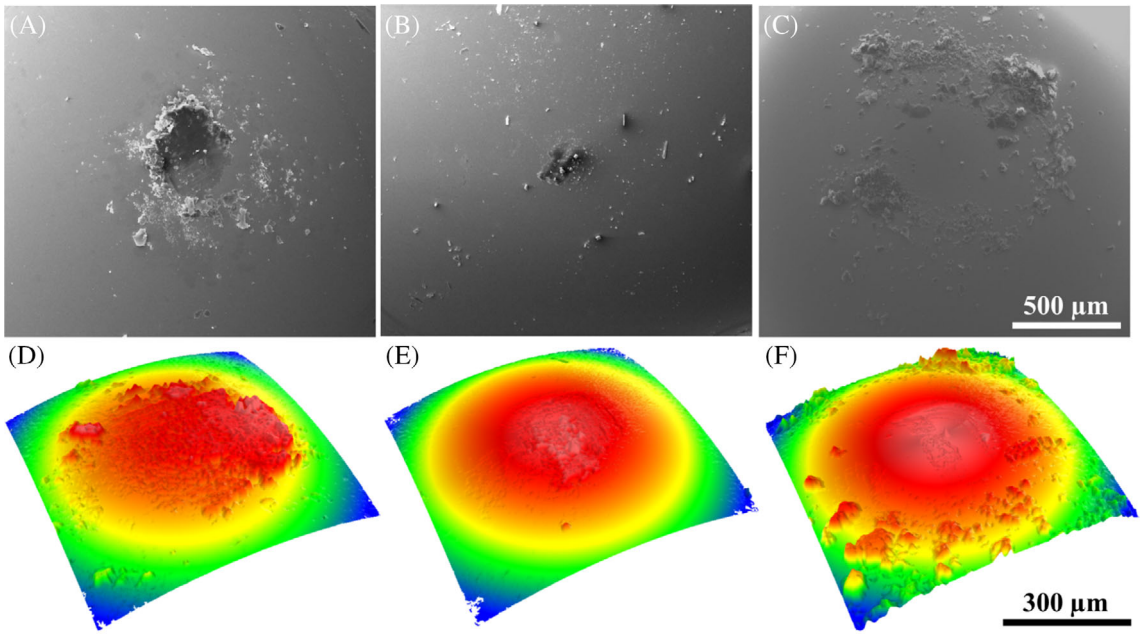

FIGURE 4 (A–C) scanning electron microscopy images and (D–F) 3D morphology of the transfer films: (A, D) polyimide, (B, E) PV-2, (C, F) PV-5.

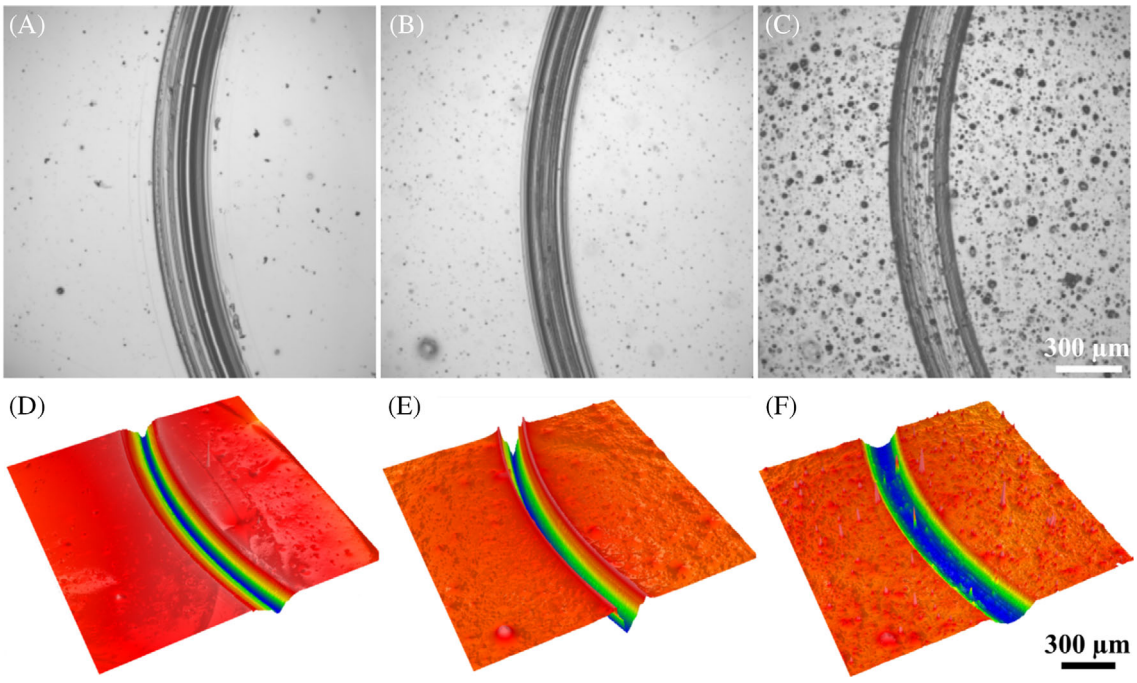

FIGURE 5 (A–C) White light interferometric fringing intensity map and (D–F) wear track of 3D: (A, D) PI, (B, E) PV-2, (C, F) PV-5.

the pristine PI specimen underwent a large area of transfer and spalling, and an adhesion effect occurred with the surface of the steel ball. This indicates that the lubrication mechanism of the pristine PI exhibits obvious characteristics of adhesive wear and fatigue wear.[26] The addition of V_2CT_x solid lubricant additive to the PI-based significantly changed its wear characteristics. Compared with the pristine PI, the groove depth of the composite was reduced, and the plastic deformation of the tribo-affected surface was alleviated (Figure S3d). The grooves and microcracks were almost eliminated when the V_2CT_x additive content wase increased from 0.4 to 0.8 wt%. At the same magnification, only slight wear was observed along the sliding direction (Figure 5E).

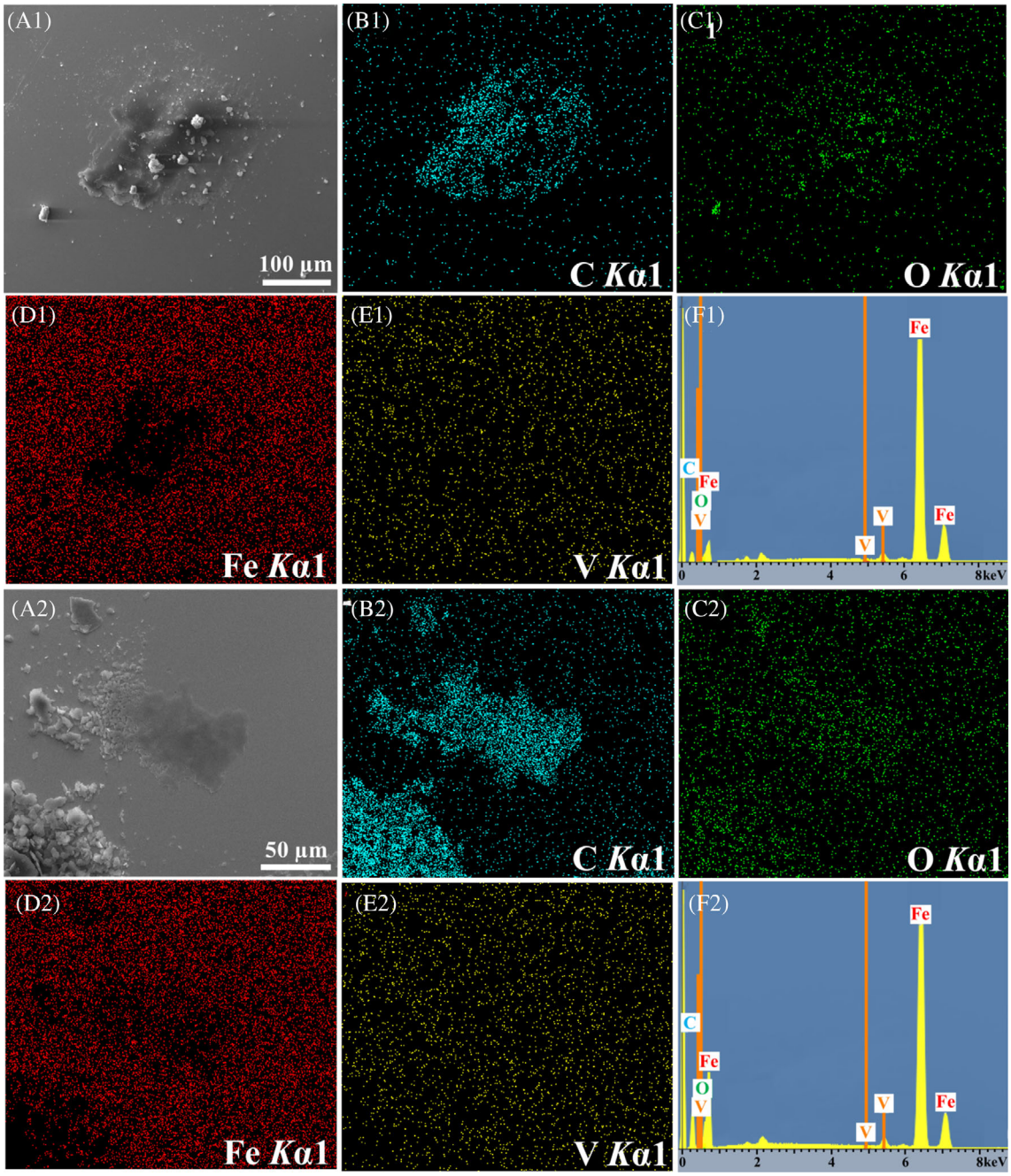

FIGURE 6 ($A_1 \sim F_1$) PV-2, ($A_2 \sim F_2$) PV-3 EDS diagram of transfer film on friction balls after friction.

However, when the filling content of V_2CT_x reached 1.2 wt%, plastic deformation of the tribo-affected surface appeared again, but the depth of the abrasion reached minimum (Figures S3e and 3C). At V_2CT_x filling contents of 1.6 and 2.0 wt%, it can be seen that the specimens were spalled by friction over a large area with serious plastic deformation. This shows abrasive wear characteristics and poor wear resistance of the specimens. Combined with these morphology diagrams, we learn that the addition of an appropriate amount of MXene improves the friction properties of PI. However, an excessive amount of MXene causes the opposite effect. This phenomenon can be explained by the fact that the relatively high content of V_2CT_x additive is not uniformly distributed in the PI-based and can weaken the bonding strength between the components of the composite and agglomeration occurs, leading to stress distortion of the nanoparticles near the agglomerates. Figure 5A–C shows the light intensity map of the tribo-affected surface of the composite film. The reflected wear marks are consistent with those obtained from the 3D white light interference surface morphology.

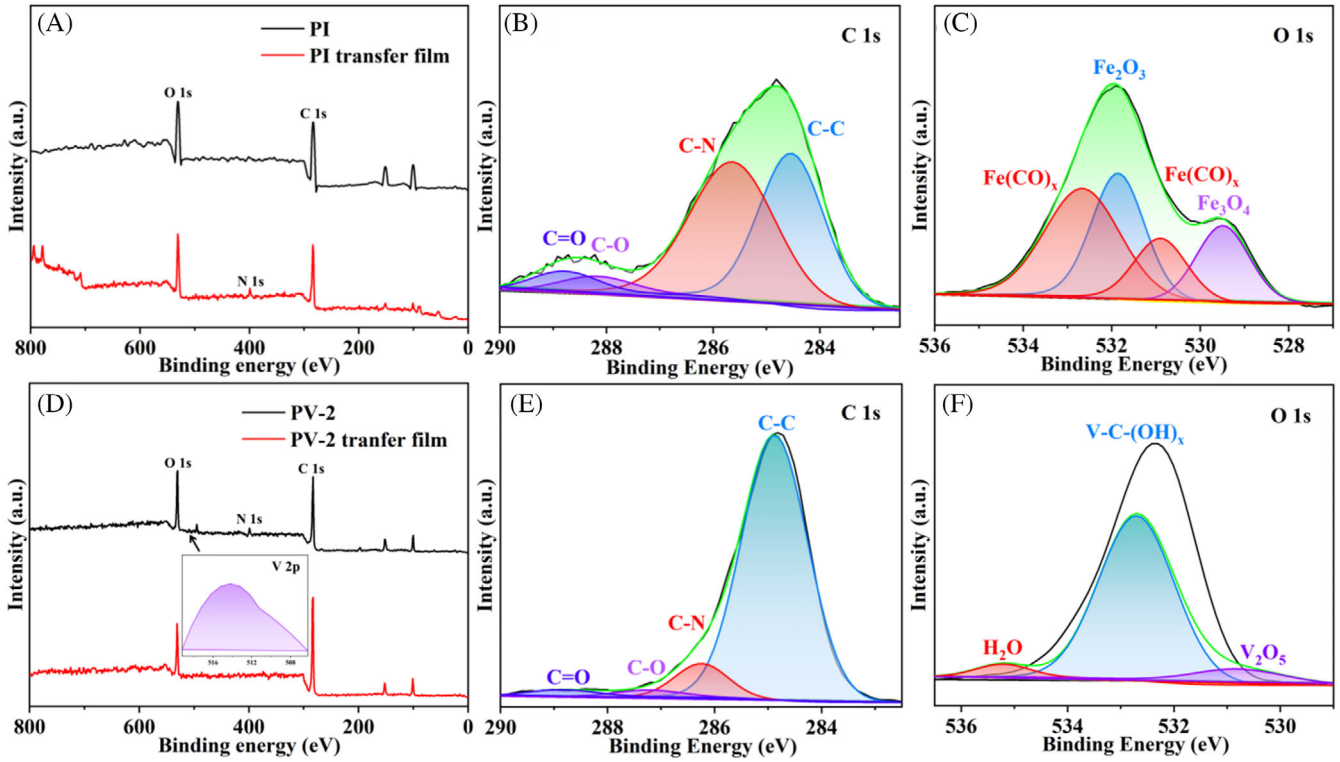

FIGURE 7 X-ray photoelectron spectroscopy (A, D) full spectrum and (B, C, E, F) fine spectra of the transfer films: (A, B, C) polyimide (PI), (D, E, F) PV-2.

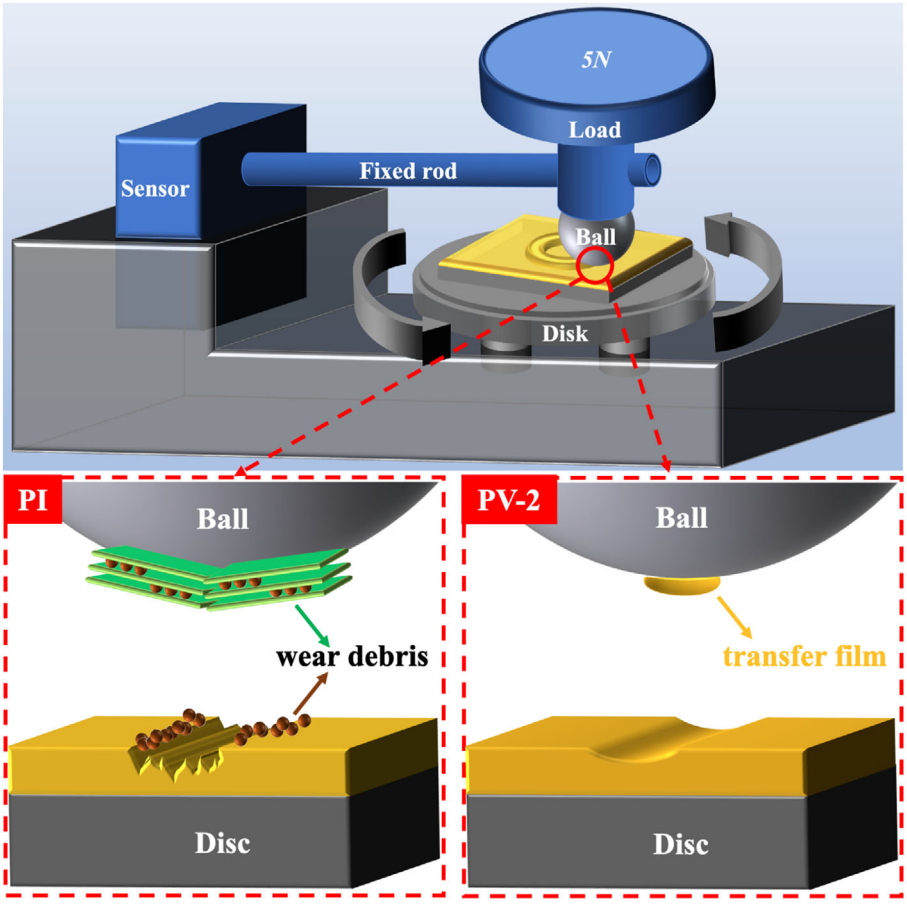

FIGURE 8 Schematic diagram of the lubrication mechanism of PI and PV-2.

3.4 | Lubrication mechanism analysis

To determine the elemental composition of the transfer film, EDS analysis was performed on the contact surface (Figure 6). The percentage of carbon atoms of the friction chemical products on the surface of the bearing steel balls after friction for PI and PV-a ($a = 1 \sim 5$) was 90.91%, 90.72%, 85.17%, 91.30%, 90.63%, and 91.28%, respectively. It is presumed that a transfer film with vanadium oxide (VO_x) as the main component was formed on the contact surface corresponding to PV-2. In addition, XPS analysis of PI and PV-2 and their transfer films on bearing steel balls after the friction process was performed. The XPS spectra of PI and PV-2 are shown in Figure 7. It can be seen that the friction chemical products of PI have iron oxides (Figure 7C). The transfer film of PV-2 after the friction has V—C—O bonds and pentavalent vanadium oxides are formed.

The lubrication mechanisms of PI and PV-2 are shown in Figure 8. It is presumed that the lubrication mechanisms of PI composites with different additive contents can be divided into three main categories: (1) Lubrication mechanism of V_2CT_x additive. At this time, the amount of added V_2CT_x is small and not easy to cause agglomeration, which makes the specific surface area of V_2CT_x larger and makes the COF low. Besides, the added V_2CT_x has an interlayer slip effect and moves in concert with the PI molecular chains, which serves to increase lubrication.[29] This mechanism usually occurs when the amount of V_2CT_x is less than 0.8 wt%. (2) Mechanism of friction transfer film formation. A relatively continuous friction-transfer film will cover the specimen, making its surface smooth and reducing the shear resistance between the composite film and the steel ball. This mechanism usually occurs when the additive content is 0.4 to 0.8 wt%. (3) Nano-micro bearing lubrication mechanism. Before the abrasive debris forms large particles, nano-micro-bearings are first formed between the friction specimens, and thus pre-abrasive wear behavior occurs. The micro-bearing reduces the contact area, thus obtaining a low degree of wear. This mechanism usually occurs at additive contents of 0.8–1.6 wt%. Overall, the tribological properties of the coating depend on the quantity and dispersion of V_2CT_x in the polymer matrix. On balance, PV-2 has the best tribological properties.

4 | CONCLUSIONS

In this study, a series of PI/V_2CT_x composites were synthesized by adjusting the additional amount of V_2CT_x MXene, a novel 2D material in the PI matrix. The WR was reduced by 43.2% when only 0.8 wt% of V_2CT_x MXene was added to the pristine PI, and 71.9% when 1.2 wt% of V_2CT_x MXene was added. Similarly, the modulation of COF could also be achieved by changing the composition of the composites. They are attributed to the excellent self-lubricating properties of V_2CT_x MXene, its good dispersion in the PI matrix, and the formation of a homogeneous polymeric friction film of inorganic–organic hybrid materials on the contact surface. V_2CT_x MXene has excellent friction reduction and anti-wear properties, and can be regarded as a promising solid lubricant additive in the field of advanced composites.

ACKNOWLEDGMENTS

This research was supported by the National Natural Science Foundation of China (51905295), the Liaoning Key Laboratory of Aero-engine Materials Tribology (LKLAMTF202304), and the Tribology Science Fund of State Key Laboratory of Tribology in Advanced Equipment (SKLTKF21B09).

CONFLICT OF INTEREST STATEMENT

There are no conflicts to declare.

DATA AVAILABILITY STATEMENT

Data available on request due to privacy/ethical restrictions.

ORCID

Xuan Yin https://orcid.org/0000-0003-3249-9814
Chunpeng Chai https://orcid.org/0000-0003-0334-9403

REFERENCES

1. Park J, Drahushuk L, Ham M, et al. Molecular interactions of polyimides with single-walled carbon nanotubes. *Polym Chem*. 2013;4(2):290-295. doi:10.1039/c2py20437a
2. Cao K, Liu G. Low-molecular-weight, high-mechanical-strength, and solution-processable telechelic poly(ether imide) end-capped with ureidopyrimidinone. *Macromolecules*. 2017; 50:2016-2023. doi:10.1021/acs.macromol.7b00156
3. Hassanzadeh-Aghdam M, Ansari R, Darvizeh A. Micromechanical modeling of thermal expansion coefficients for unidirectional glass fiber-reinforced polyimide composites containing silica nanoparticles. *Compos Part A*. 2017;96:110-121. doi:10.1016/j.compositesa.2017.02.015
4. Kurosawa T, Higashihara T, Ueda M. Polyimide memory: a pithy guideline for future applications. *Polym Chem*. 2013;4(1): 16-30. doi:10.1039/c2py20632c
5. Nayak L, Rahaman M, Aldalbahi A, Chaki TK, Khastgir D. Polyimide-carbon nanotubes nanocomposites: electrical conduction behavior under cryogenic condition. *Polym Eng Sci*. 2017;57(3):291-298. doi:10.1002/pen.24412
6. Olariu MA, Hamciuc C, Asandulesa M, et al. Study on highly thermostable low-k polymer films based on fluorene-containing polyetherimides. *Polym Eng Sci*. 2021;61(10):2639-2652. doi:10.1002/pen.25792

7. Guo Y, Xu G, Yang X, et al. Significantly enhanced and precisely modeled thermal conductivity in polyimide nanocomposites with chemically modified graphene via in situ polymerization and electrospinning-hot press technology. *J Mater Chem C*. 2018;12:3004-3015. doi:10.1039/c8tc00452h
8. Chen Y, Li D, Yang W, Xiao C, Wei M. Effects of different amine-functionalized graphene on the mechanical, thermal, and tribological properties of polyimide nanocomposites synthesized by in situ polymerization. *Polymer*. 2018;140:56-72. doi:10.1016/j.polymer.2018.02.017
9. Yanming W, Tingmei W, Qihua W. Effect of molecular weight on tribological properties of thermosetting polyimide under high temperature. *Tribol Intern*. 2014;78:47-59. doi:10.1016/j.triboint.2014.04.031
10. Roy A, Mu L, Shi Y. Tribological properties of polyimide-graphene composite coatings at elevated temperatures. *Prog Org Coat*. 2020;142:105602. doi:10.1016/j.porgcoat.2020.105602
11. Yang M, Zhang C, Su G, Dong Y, Mekuria T, Lv Q. Preparation and wear resistance properties of thermosetting polyimide composites containing solid lubricant fillers. *Mater Chem Phys*. 2020;241:122034. doi:10.1016/j.matchemphys.2019.122034
12. Min Y, Kang K, Kim D. Development of polyimide films reinforced with boron nitride and boron nitride nanosheets for transparent flexible device applications. *Nano Res*. 2018;11(5):2366-2378. doi:10.1007/s12274-017-1856-0
13. Li X, Jia X, Xiao Q, et al. CuO nanowires uniformly grown on carbon cloth to improve mechanical and tribological properties of polyimide composites. *Mater Chem Phys*. 2022;281:125852. doi:10.1016/j.matchemphys.2022.125852
14. Naguib M, Kurtoglu M, Presser V, et al. Two-dimensional nanocrystals produced by exfoliation of Ti_3AlC_2. *Adv Mater*. 2011;23(37):4248-4253. doi:10.1002/adma.201102306
15. Lipatov A, Lu H, Alhabeb M, et al. Elastic properties of 2D $Ti_3C_2T_x$ MXene monolayers and bilayers. *Sci Adv*. 2018;4(6):eaat0491. doi:10.1126/sciadv.aat0491
16. Borysiuk V, Mochalin V, Gogotsi Y. Bending rigidity of two-dimensional titanium carbide (MXene) nanoribbons: a molecular dynamics study. *Comput Mater Sci*. 2018;143:418-424. doi:10.1016/j.commatsci.2017.11.028
17. Meng Y, Xu J, Jin Z, Prakash B, Hu Y. A review of recent advances in tribology. *Friction*. 2020;8(2):221-300. doi:10.1007/s40544-020-0367-2
18. Zhang H, Wang L, Chen Q, et al. Preparation, mechanical and anti-friction performance of MXene/polymer composites. *Mater Design*. 2016;92:682-689. doi:10.1016/j.matdes.2015.12.084
19. Marian M, Song G, Wang B, et al. Effective usage of 2D MXene nanosheets as solid lubricant–influence of contact pressure and relative humidity. *Appl Surf Sci*. 2020;531:147311. doi:10.1016/j.apsusc.2020.147311
20. Huang S, Mutyala K, Sumant A, Mochalin V. Achieving superlubricity with 2D transition metal carbides (MXenes) and MXene/graphene coatings. *Mater Today Adv*. 2021;9:100133. doi:10.1016/j.mtadv.2021.100133
21. Liang Z, Huimin Q, Yang L, Jiaxin Y, Baogang G, Ding Z. Ti_3C_2 MXene induced high tribological performance of polyimide/polyurea copolymer at a wide temperature range. *Appl Surf Sci*. 2022;608:155157. doi:10.1016/j.apsusc.2022.155157
22. Zheng Z, Guo C, Wang E, et al. The oxidation and thermal stability of two-dimensional transition metal carbides and/or carbonitrides (MXenes) and the improvement based on their surface state. *Inorg Chem Front*. 2021;8(9):2164-2182. doi:10.1039/d1qi00041a
23. Zhou X, Guo Y, Wang D, Xu Q. Nano friction and adhesion properties on Ti_3C_2 and Nb_2C MXene studied by AFM. *Tribol Intern*. 2021;153:106646. doi:10.1016/j.triboint.2020.106646
24. Yin X, Chen H, Jiang L, et al. Effects of polyacrylic acid molecular weights on V_2C-MXene nanocoatings for obtaining ultralow friction and ultralow wear in an ambient working environment. *Phys Chem Chem Phys*. 2022;24(44):27406-27412. doi:10.1039/d2cp03639h
25. Zhang Y, Lu W, Zhou J, Sun D, Li H. The multiple synthesis of layered V_2CT_x-MXene composites with enhanced electrochemical properties. *J Alloys Compd*. 2022;929:167276. doi:10.1016/j.jallcom.2022.167276
26. Ogura T, Saito Y, Higashihara T, Ueda M. Formation of spherical nanoparticles in poly (amic acid) films. *Polym Chem*. 2012;3:2165-2169. doi:10.1039/c2py20093g
27. Qi HM, Hu C, Zhang G, Yu JX, Zhang YF, He HT. Comparative study of tribological properties of carbon fibers and aramid particles reinforced polyimide composites under dry and sea water lubricated conditions. *Wear*. 2019;436:203001. doi:10.1016/j.wear.2019.203001
28. Wan C, Yao C, Li J, et al. Friction and wear behavior of polyimide matrix composites filled with nanographite. *J Appl Polym Sci*. 2022;139(18):e52058. doi:10.1002/app.52058
29. Weber B, Suhina T, Brouwer A, Bonn D. Frictional weakening of slip interfaces. *Sci Adv*. 2019;5(4):eaav7603. doi:10.1126/sciadv.aav7603

SUPPORTING INFORMATION

Additional supporting information can be found online in the Supporting Information section at the end of this article.

How to cite this article: Jin L, Wang X, Huang Y, et al. Lubrication mechanism of polyimide/V_2CT_x MXene composites based on surface chemistry. *Polym Compos*. 2023;1-10. doi:10.1002/pc.27689